Mon. Not. R. Astron. Soc. **298,** L49–L53 (1998)

# SCUBA imaging of the NGC 7331 dust ring

S. Bianchi,[1] P. B. Alton,[1] J. I. Davies[1] and M. Trewhella[2]
[1]*Department of Physics and Astronomy, University of Wales Cardiff, PO Box 913, Cardiff CF2 3YB*
[2]*IPAC, M.S. 100-22 Caltech, Pasadena, CA 91125, USA*

Accepted 1998 June 17. Received 1998 June 12; in original form 1998 April 24

**ABSTRACT**

We present observations of the spiral galaxy NGC 7331 using the Submillimetre Common User Bolometer Array (SCUBA) on the James Clark Maxwell Telescope. We have detected a dust ring of 45 arcsec radius (3.3 kpc) at wavelengths of 450 and 850 μm. The dust ring is in good correspondence with other observations of the ring in the mid-infrared (MIR), CO and radio continuum, suggesting that the observed dust is associated with molecular gas and star formation. A $B-K$ colour map shows an analogous ring structure with an asymmetry about the major axis, consistent with the extinction being produced by a dust ring. The derived temperature of the dust lies between 16 and 31 K and the gas-to-dust ratio lies between 150 and 570, depending on the assumed dust emission efficiency index ($\beta = 1.5$ or 2).

**Key words:** dust, extinction – galaxies: individual: NGC 7331 – galaxies: ISM – galaxies: structure.

## 1 INTRODUCTION

Modelling of *COBE*– DIRBE observation of our Galaxy has shown that dust at $T < 22$ K associated with neutral and molecular gas is responsible for most of the emission (55–85 per cent) in the far-infrared (FIR) (Sodroski et al. 1994; Sodroski et al. 1997). Reach et al. (1995), analysing *COBE*– FIRAS spectral data, find that Galactic emission between 100 and 300 μm is predominantly from dust at $T = 16$–23 K. This range of temperatures is in agreement with theoretical calculations for classical grains heated by the interstellar radiation field (ISRF) (Disney, Davies & Phillipps 1989).

In external galaxies, dust temperatures have been mainly measured using *IRAS* fluxes at 60 and 100 μm. *IRAS* can only trace warm dust at $T \gtrsim 30$ K (Devereux & Young 1990). This is mainly associated with star forming regions, as illustrated by the strong correlation between Hα and *IRAS* FIR emission (Devereux 1995). Gas-to-dust ratios derived from *IRAS* are a factor of 10 larger than the Galactic value (Devereux & Young 1990). Assuming that the Galaxy is typical of spirals, the discrepancy can be explained by a colder dust component ($T \approx 15$ K) that contributes to the bulk of the mass, without adding a lot of flux in the window observed by *IRAS* (Devereux & Young 1990). This is because of the strong dependence of emission on temperature ($\propto T^{4+\beta}, \beta = 1-2$).

Estimates of the temperature of the main dust component depend on the availability of data at λ >100 μm. Recently, Alton et al. (1998a) have measured $\langle T \rangle \approx 20$ K for a sample of seven spiral galaxies, using *ISO*PHOT 200-μm maps combined with HiRes *IRAS* maps at 100 μm, 10 K lower than the temperatures measured using *IRAS* HiRes 60-μm data. The mean gas-to-dust ratio is then ≈230, closer to the canonical Galactic value of 160 (Sodroski et al. 1994). Newly available FIR maps, despite their low resolution (117 arcsec for *ISO*PHOT data) have revealed that the spatial distribution of dust is more extended than that of the *IRAS* and *K*-band (stellar) emission (Alton et al. 1998a; Davies et al. 1998).

In this Letter we describe submillimetre (submm) observations of NGC 7331 with SCUBA. Maps produced by SCUBA have a far higher resolution than *ISO*PHOT and HiRes *IRAS* long-wavelength observations and give us detailed spatial information about the extent of cold dust. NGC 7331 is an Sb galaxy (de Vaucouleurs et al. 1991) at a distance of 15.1 Mpc (Hughes et al. 1998), giving an apparent scale of 73 pc arcsec$^{-1}$.

NGC 7331 shows a ring structure in CO emission (Young & Scoville 1982; von Linden et al. 1996; Tosaki & Shioya 1997), radio continuum (Cowan, Romanishin & Branch 1994) and MIR images from *ISO*CAM ($6.75\,\mu\text{m} < \lambda < 15\,\mu\text{m}$; Smith 1998). Smith (1998) also shows that these observations are in good correspondence with each other, indicating the presence of a molecular gas and dust ring of radius ≈45 arcsec (3 kpc). There is also a good match with Hα+[N II] features (Pogge 1989). The central region (radius ≈2 arcmin) is partially depleted of neutral hydrogen (Bosma 1981) whilst the molecular gas contributes to 70 per cent of the total gas mass inside the optical radius (Devereux & Young 1990). A major axis profile at 100 μm obtained with the Kuiper Airborne Observatory (KAO) (Smith & Harvey 1996) shows a flat-topped FIR distribution (FWHM ≈ 35 arcsec), but very little structure can be seen in the HiRes *IRAS* maps or in the 200-μm *ISO*PHOT observations of Alton et al. (1998a) (FWHM ≳ 50 arcsec).

The ring may be the result of long-term dynamical evolution driven by a bar instability, as proposed by von Linden et al. (1996). Tosaki & Shioya (1997) relate the ring to the post-starburst status of the galaxy: the central gas is consumed in the long evolution after the starburst event.

## 2 OBSERVATIONS AND DATA REDUCTION

NGC 7331 was observed at JCMT with SCUBA on 1997 October 20, 22 and 24. SCUBA consists of two bolometer arrays able to image simultaneously a region of sky of about 2.3 arcmin in diameter: the *short-wavelength array*, optimized for observing at 450 μm (91 elements), and the *long-wavelength array*, optimized at 850 μm (37 elements). To sample the field of view fully with both the arrays, the secondary mirror is moved in a 64-point jiggle pattern. For each jiggle position the integration time is 1 s. Simultaneously, the secondary mirror is also chopping with a frequency of 7 Hz to remove the sky background. Every 16 steps of the jiggle pattern, the telescope nods, to remove slowly varying atmospheric gradients. We used a chop throw of 180 arcsec perpendicular to the major axis of NGC 7331.

We frequently determined the transparency of the atmosphere during each night by measuring sky emission at several elevations. Sky conditions were stable during most of the observing run with zenith optical depths of $\tau_{450} = 0.6$–$0.7$ and $\tau_{850} = 0.13$–$0.15$. During the first night atmospheric opacity was higher, with $\tau_{450} > 3$ and $\tau_{850} = 0.5$. The telescope pointing was checked every hour against a bright point source close to our target: rms pointing errors were $\approx$ 3 arcsec in both azimuth and elevation. Several images of Uranus were taken for photometric calibration.

Data reduction was carried out using the Starlink package SURF (Jenness & Lightfoot 1997; Sandell 1997). After subtracting the *off-source* signal, images were flat-fielded and corrected for atmospheric extinction. Noisy bolometers were masked. Each image was corrected for systematic noise variations using stable bolometers that appeared free of source emission. Spikes from transient detections were removed by applying a $3\sigma$ clip.

A calibration constant for each night was computed from the Uranus maps. Comparing data for each night we derived relative errors in calibration of 14 and 7 per cent, for 450 and 850 μm respectively. Uranus images were also used to measure the beam size and the contribution of side lobes. The measured HPBW is 10 arcsec at 450 μm and 15 arcsec at 850 μm. The side lobes can introduce quite large systematic errors: for example, 20 per cent of the emission of a point source goes in the side lobes for the longer wavelength and 60 per cent for the shorter wavelength. In the following, values of integrated flux are corrected for the side-lobe pickup.

A total of 15 images at 450 μm and 19 images at 850 μm were re-sampled to an equatorial reference frame, using pixels of size 3 and 5 arcsec, respectively. The final map covers an area of 3.3 arcmin × 5.8 arcmin. The total *on-source* integration times for the central part of the image are 5700 and 8300 s. Maps are shown in Fig. 1; contours with signal-to-noise ratio (S/N) ≥3 are overplotted. The short-wavelength image clearly shows a poorer signal-to-noise ratio, mainly because of the higher emissivity of the sky at 450 μm compared with that at 850 μm: the sky noise is 80 mJy beam$^{-1}$ at 450 μm and 8 mJy beam$^{-1}$ at 850 μm.

In this work we have also used *B*- and *K*-band observations. Images were obtained from the Skinakas observatory Crete (in *B*) and at the Wyoming Infrared Observatory (in *K*). The optical and NIR data were reduced and calibrated in the standard way (Trewhella 1997). The PSF has a FWHM of 1.5 arcsec for the *B*-band image and 2.5 arcsec for the *K*-band image. Optical images were aligned in a RA/Dec. frame using field stars in the *HST* guide star catalogue. The peak emission in the *B*-band image occurs at RA = $22^{\rm h}\,37^{\rm m}\,04^{\rm s}$, Dec=$34^\circ\,24'\,55\overset{''}{.}5$ (J2000); these coordinates are within 1.5 arcsec of the optical and radio emission centres given by Cowan et al. (1994). SCUBA images were aligned by assuming the *B* peak as the centre of the frame. Images in the *B* band and $B-K$ colour are shown in Fig. 1. The $B-K$ colour image has a photometric accuracy of 0.2 mag.

## 3 RESULTS AND DISCUSSION

Our 850-μm image (Fig. 1, top right) clearly shows a ring structure, of ≈ 90 arcsec × 30 arcsec (radius≈ 45 arcsec, corresponding to 3.3 kpc). This submm ring matches MIR observations, and therefore CO, radio continuum and Hα+[NII] observations, as shown in Smith (1998).

The brightest parts of the ring are on the north and south sides, where intensity peaks are at almost the same value (95 mJy beam$^{-1}$, S/N≈ 12). The east and west side of the ring are less bright and appear clumpy. As suggested by von Linden et al. (1996) for the CO ring, this morphology may well be a result of the inclined view. There are also two smaller structures attached to the north and south sources [seen in our image at positions (5, 60) and (20, −50), respectively]. The south one, the brightest, is associated with the origin of one of the spiral arms in our optical image (Fig. 1, bottom left). There is no evidence for a central source, contrary to the MIR images (Smith 1998). The ring is also visible in the 450-μm image (Fig. 1, top left) despite the poorer signal. When smoothed to the long-wavelength resolution, the same structures can be seen.

Radial surface-brightness profiles were produced for the 850-μm and smoothed 450-μm images, averaging over elliptic annuli. We have adopted a disc inclination of 74° and PA = 167° (Garcia-Gomez & Athanassoula 1991). The two profiles can be followed out to 150 arcsec from the centre (both images with S/N > 1), and they appear similar (Fig. 2).

Using this last aperture, we have computed the integrated fluxes: we obtain a flux of 13.4 Jy for 450 μm and 1.9 Jy for 850 μm. The ratio between the fluxes is therefore $7.0 \pm 1.0$, where the error is mostly caused by the uncertainties in the calibration. From this ratio the average dust temperature can be computed, if the dependence of dust emissivity $Q_{\rm em}$ on wavelength λ is known. It is generally assumed that $Q_{\rm em} \propto \lambda^{-\beta}$, with $\beta$ increasing from 1 to 2 going from the MIR to the FIR and submm (Hildebrand 1983). Fits of the Galactic FIR–submm spectrum (Reach et al. 1995) suggest a value $\beta = 2$ for $\lambda > 200$ μm. Millimetre/submm observations of the Galactic plane and cirrus (Masi et al. 1995) emission are better described by $\beta = 1.5$. Using $\beta = 2$ we derive $T = 16 \pm 3$ K ($T = 31 \pm 10$ K for $\beta = 1.5$). The temperature obtained using $\beta = 2$ agrees very well with values for high-latitude dust emission in the Galaxy (Reach et al. 1995). It is interesting to note that a greybody model with $\beta = 1$ cannot be fitted to the data. This is also confirmed by SCUBA observations of NGC 891 (Alton et al. 1998b).

The dust temperature was also derived using the KAO 100-μm observations presented by Smith & Harvey (1996). The image at 850 μm was smoothed to the KAO resolution (31 arcsec × 41 arcsec) and a profile along the major axis was produced, with the same orientation as the one shown in their fig. 5. In the central 100 arcsec, where the KAO profile appears flat, the average flux density per bolometer at 100 μm is 29 Jy. In the same region the average value for the 850-μm flux is 60 mJy beam$^{-1}$. From the ratio we derived $T = 23$ K $\pm$ 2 for $\beta = 2$ ($T = 29$ K $\pm$ 3 for $\beta = 1.5$). Alton et al. (1998a) 100-μm fluxes and *ISO* 200-μm fluxes give values of $T = 17$ K for $\beta = 2$ and $T = 19$ K for $\beta = 1.5$.

The correspondence between the submm ring and other observations suggests that the dust emission is associated with the

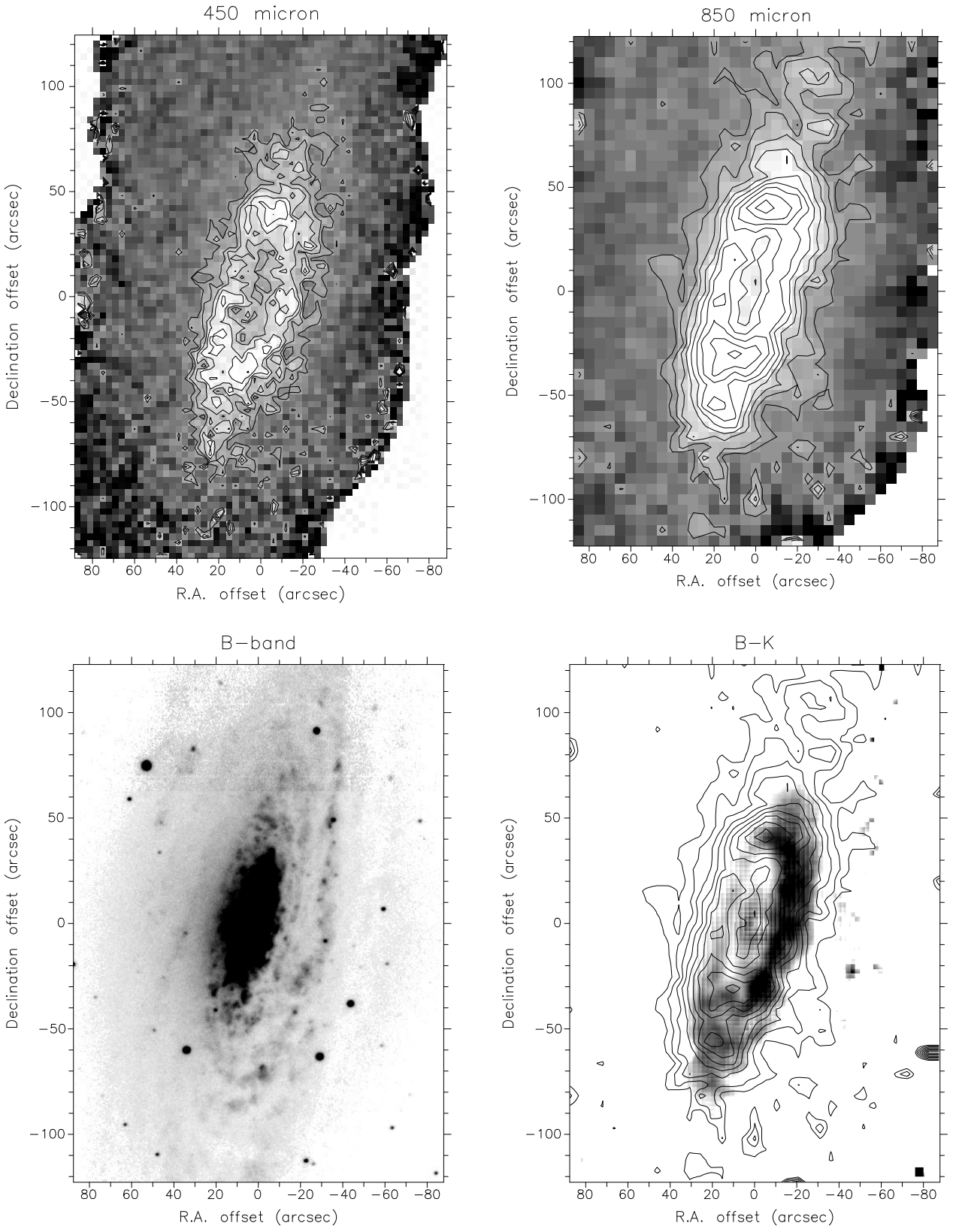


**Figure 1.** 450-μm (top left), 850-μm (top right) *B*-band (bottom left) and $B - K$ (bottom right) maps of NGC 7331. For submm images, contours are overlayed at integer values of the S/N ratio, starting from S/N = 3 (for the 450-μm image this corresponds to isophotes every 80 mJy beam$^{-1}$ starting from 240 mJy beam$^{-1}$; for the 850-μm image, isophotes every 8 mJy beam$^{-1}$ starting from 24 mJy beam$^{-1}$). Contours at 850 μm are also overlayed on the $B - K$ image.

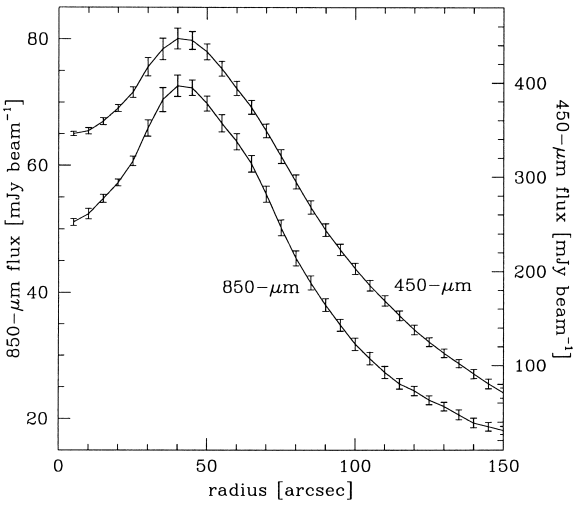


**Figure 2.** Elliptically averaged surface brightness profiles for 850- and 450-μm images. Isophote geometrical parameters are described in the text. Error bars represent the standard deviation of the mean inside each elliptical annulus.

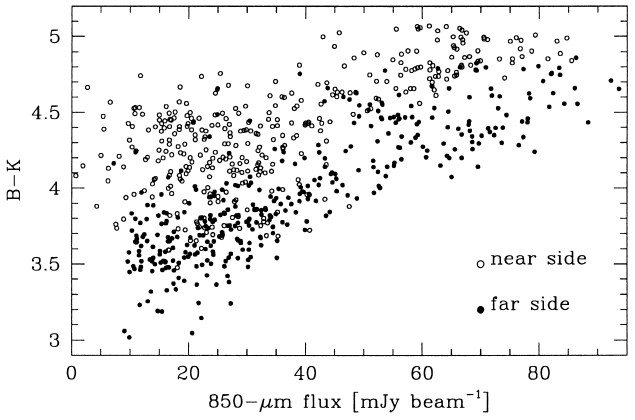


**Figure 3.** Correlation between pixels in a $B-K$ smoothed image and 850-μm image, inside a 100 arcsec × 50 arcsec region centred on the galaxy. Filled circles refer to the far side of the galaxy (i.e. east side) and open circles to the near side (i.e. west side). The ring structure evident in the 850-μm image (Fig. 1) corresponds to fluxes larger than 60 mJy beam$^{-1}$. Each data point has a random error of ≈ 0.05 mag.

molecular gas. Indeed, the values of dust temperature we have presented here are consistent with those of the dust component associated with the molecular gas in the Galaxy (Sodroski et al. 1997).

The $B-K$ map is shown in Fig. 1, bottom right, with the 850-μm contour superimposed. A ring structure can be seen in the colour image, in excellent correspondence with the submm image. The ring is delimited on the east and west sides by regions with a redder colour with respect to the central one. The colour on the west side is also redder than on the east. The asymmetry and the central gap, first observed in NIR colors by Telesco, Gatley & Steward (1982), can be explained by a bulge obscured by an inclined dust ring. On the west side (the closer one) most of the bulge is behind the dust ring so that bulge light is more extinguished and therefore redder than on the east side (the far one). Because of the relative lack of dust in the middle of the structure, bulge light from the central region appears bluer.

To compare $B-K$ with 850-μm emission, the colour image was smoothed to a resolution of 15 arcsec and rebinned on 5-arcsec pixels. We have then plotted $B-K$ versus the 850-μm flux for each pixel in an elliptic region of ≈ 100 arcsec × 50 arcsec (Fig. 3). A clear trend is evident: for the same 850-μm flux, the closer part of the galaxy is systematically redder than the far one, by 0.5 mag. This is true both for the regions with high flux (i.e. high dust column density) that define the ring and for regions external to the ring. Bulge light extinguished by a more extended dust disc may be the reason for the colour asymmetry of these outer regions. As a check, we repeated the correlation using pixels of 15 arcsec, but the conclusions are the same: our results are thus independent of a possible misalignment of the colour and submm images, which we estimate to be at most 2.5 arcsec.

$B-K$ is more sensitive than optical colours to the presence of dust (Block et al. 1994), because of the high ratio between extinction in the $B$ and $K$ bands [≈14, using a Galactic extinction law (Whittet 1992)]. Even so, deriving the dust content from the colour image is quite difficult. First, an a priori knowledge of the *intrinsic* colour distribution is required to quantify the *reddening*; secondly, the relative distribution of dust and stars must be known to infer, by means of a radiative transfer model, the relation between the reddening and the optical depth (or the dust column density). These two steps are obviously coupled together (see for example Xilouris et al. 1997, 1998).

We can easily obtain a lower limit to the optical depth of the ring. We assume the thickness of the dust structure to be negligible so that dust acts like an internal *screen* for light emitted by a spheroidal bulge. On the near part of the galaxy we assume that all the light is extinguished (i.e. the bulge is all behind the screen). On the far side the situation is reversed, with none of the bulge light extinguished. These assumptions are justified by the high inclination of NGC 7331 and by the luminous bulge, which has an effective radius similar to the ring (31 arcsec; Boroson 1981). Within this model, the $B-K$ on the far side can be regarded as the intrinsic colour of the bulge, and the difference between the two halves as the colour excess resulting from dust extinction. From the difference in $B-K$ of 0.5 mag we can thus derive an optical depth in the $V$ band of ≈0.4, if a Galactic extinction law is assumed. In reality the dust distribution will have a finite thickness; also, scattering and clumpiness should be considered. Inclusion of these features would have the effect of reducing the extinction for a given quantity of dust (Boissé & Thoraval 1996; Witt & Gordon 1996).

Submm images permit us to derive the $V$-band optical depth of the dust distribution in a way independent of geometry. The optical depth $\tau_V$ can be related to the flux at $\lambda = 850$ μm using the formula (Hildebrand 1983)

$$\tau_V = \frac{1}{2}\left(\frac{Q_{UV}}{Q_{\lambda_0}}\right)\left(\frac{\lambda}{\lambda_0}\right)^{\beta}\frac{I_\lambda}{B_\lambda(T)},$$

where $T$ is the temperature of the dust, $I_\lambda$ is the intensity (i.e. the flux per beam divided by the integrated beam size), $B_\lambda(T)$ is the Planck function and $\beta$ the emissivity index. $Q_{UV}$ is the extinction efficiency in the ultraviolet range (1500–3000 Å), while $Q_{\lambda_0}$ is the emission efficiency at a reference wavelength $\lambda_0$. The ratio $Q_{UV}/Q_{\lambda_0}$ is quite uncertain, but from Hildebrand (1983) and Casey (1991) we have derived a mean value $Q_{UV}/Q_{\lambda_0} \approx 1200$ at $\lambda_0 = 125$ μm for $\beta = 2$. The value of $Q_{UV}/Q_{\lambda_0}$ for $\beta = 1.5$ has been roughly derived from data in Casey (1991): we use $Q_{UV}/Q_{\lambda_0} = 2100$ at $\lambda_0 = 125$ μm. Typically, values of $Q_{UV}/Q_{\lambda_0}$ have uncertainties of a factor of 2–3. The factor of 1/2 comes from assuming $\tau_{UV}/\tau_V = 2$ (Casey 1991). For the ring (mean flux of 70 Jy beam$^{-1}$) we obtain face-on optical

depths of $\tau_V = 2.4$ and 9.3, for $\beta = 1.5$ and 2 respectively. At the $1\sigma$ isophote, $\tau_V = 0.4$ and 0.9. Uncertainties in $\tau_V$ are quite large, because of the uncertainties in both $T$ and the value $Q_{UV}/Q_{\lambda_0}$. Using temperatures derived with the help of KAO data, optical depths are $\tau_V = 2.6$ and 5.4, for $\beta = 1.5$ and 2 respectively. Telesco et al. (1982) derived $\tau_V \approx 3$ for the reddest part of the galaxy.

The mass column density of dust can be derived from the optical depth. Adopting a mean dust grain radius of 0.1-μm, a density of $3\,\mathrm{g\,cm^{-3}}$ and an extinction efficiency in the $V$ band of 1.5 (Hildebrand 1983; Casey 1991), we have obtained ring column densities of $N_\mathrm{d} = 0.3$ and $1.1\,\mathrm{M_\odot\,pc^{-2}}$ for $\beta = 1.5$ and 2, respectively ($N_\mathrm{d} = 0.04$ and $0.1\,\mathrm{M_\odot\,pc^{-2}}$ at $1\sigma$ level). From CO maps of the east and west sides of the ring, Tosaki & Shioya (1997) have deduced a mean mass column density for the molecular gas of $150\,\mathrm{M_\odot\,pc^{-2}}$ (we note here that there are possible uncertainties related to the smaller beam size of their observations). An atomic gas column density of $20\,\mathrm{M_\odot\,pc^{-2}}$ has been derived from Bosma (1981) for the position of the ring. The total gas column density for the ring is thus $N_\mathrm{g} = 170\ \mathrm{M_\odot\ pc^{-2}}$. The gas-to-dust mass ratio is then 150 for $\beta = 2$ (570 for $\beta = 1.5$). The value derived for $\beta = 2$ is much closer to the Galactic value than *IRAS*-based ratios (Devereux & Young 1990) and in agreement with *ISO*-based determinations (Alton et al. 1998a; Davies et al. 1998), as well as with optical–NIR radiative transfer models (Xilouris et al. 1997, 1998).

The dust mass inside 150 arcsec is $M_\mathrm{d} = 4 \times 10^7\ \mathrm{M_\odot}$ for $\beta = 2$ ($M_\mathrm{d} = 1 \times 10^7\ \mathrm{M_\odot}$ for $\beta = 1.5$). From Alton et al. (1998a) data, covering a larger area ($\approx$ 10 arcmin), we can derive a dust mass of $M_\mathrm{d} = 1.2 \times 10^8\,\mathrm{M_\odot}$ (for both values of $\beta$). Therefore the total mass is at least three times larger than the one we have derived here. This shows that there is a large and diffuse component of dust (> 70 per cent in mass) that is not associated with the molecular ring. It is interesting to note that an extended dust distribution may be the reason why some millimetre and submm observations (Eales, Wynn-Williams & Duncan 1989; Clements, Andreani & Chase 1993) have failed to detect cold dust, because of the small size of the bolometers used compared with the extent of the dust (Clements et al. 1993).

## ACKNOWLEDGMENTS

We are grateful to Iain Coulson at JCMT for his help and support during observations and data reduction. It is also a pleasure to thank Beverly Smith for providing us with KAO data, Manolis Xilouris for the *B*-band image and Harley Thronson for help with the *K*-band data. This paper was based on observations at the James Clerk Maxwell Telescope. JCMT is operated by the Joint Astronomy Centre on behalf of the Particle Physics and Astronomy Research Council of the United Kingdom, the Netherlands Organization for Scientific Research and the National Research Council of Canada.

## REFERENCES

Alton P. B., Trewhella M., Davies J. I., Evans R., Bianchi S., Gear W., Thronson H., Valentijn E., Witt A., 1998a, A&A, 335, 807
Alton P. B., Bianchi S., Rand R. J., Xilouris E. M., Davies J., Trewhella M., 1998b, ApJ, submitted
Block D. L., Witt A. N., Grosbøl P., Stockton A., Moneti A., 1994, A&A, 288, 383
Boissé P., Thoraval S., 1996, in Block D. L., Greenberg J. M., eds, New Extragalactic Perspectives in the New South Africa. Kluwer, Dordrecht, p. 187
Boroson T., 1981, ApJS, 46, 32
Bosma A., 1981, AJ, 86, 1791
Casey S. C., 1991, ApJ, 371, 183
Clements D. L., Andreani P., Chase S. T., 1993, MNRAS, 261, 299
Cowan J. J., Romanishin W., Branch D., 1994, ApJ, 436, L139
Davies J. I., Alton P. B., Trewhella M., Evans R., Bianchi S., 1998, MNRAS, submitted
de Vaucouleurs G., de Vaucouleurs A., Corwin H. G., Buta R. J., Paturel G., Fouque P., 1991, Third Reference Catalogue of Bright Galaxies. Springer, New York
Devereux N. A., 1995, in Davies J. I., Burstein D., eds, Proc. NATO ARW, NATO ASI Ser. 469, The Opacity of Spiral Disks. Kluwer, Dordrecht, p. 269
Devereux N. A., Young J. S., 1990, ApJ, 359, 42
Disney M., Davies J., Phillipps S., 1989, MNRAS, 239, 939
Eales S. A., Wynn-Williams C. G., Duncan W. D., 1989, ApJ, 339, 859
Garcia-Gomez C., Athanassoula E., 1991, A&AS, 89, 159
Hildebrand R. H., 1983, QJRAS, 24, 267
Hughes S. M. G. et al., 1998, ApJ, 501, 32
Jenness T., Lightfoot J. F., 1997, Starlink User Note 216.1
Masi S. et al., 1995, ApJ, 452, 253
Pogge R. W., 1989, ApJS, 71, 433
Reach W. T. et al., 1995, ApJ, 451, 188
Sandell G., 1997, Starlink Cookbook 11.1
Smith B. J., 1998, ApJ, 500, 181
Smith B. J., Harvey P. M., 1996, ApJ, 468, 139
Sodroski T. J. et al., 1994, ApJ, 428, 638
Sodroski T. J., Odegard N., Arendt R. G., Dwek E., Weiland J. L., Hauser M. G., Kelsall T., 1997, ApJ, 480, 173
Telesco C. M., Gatley I., Steward J. M., 1982, ApJ, 263, L13
Tosaki T., Shioya Y., 1997, ApJ, 484, 664
Trewhella M., 1997, PhD thesis, Univ. Wales Cardiff
von Linden S., Reuter H.-P., Heidt J., Wielebinski R., Pohl M., 1996, A&A, 315, 52
Whittet D. C. B., 1992, Dust in the Galactic Environment. IOP, Bristol
Witt A. N., Gordon K. D., 1996, ApJ, 463, 681
Xilouris E. M., Kylafis N. D., Papamastorakis J., Paleologou E. V., Haerendel G., 1997, A&A, 325, 135
Xilouris E. M., Alton P. B., Davies J. I., Kylafis N. D., Papamastorakis J., Trewhella M., 1998, A&A, 331, 894
Young J. S., Scoville N., 1982, ApJ, 260, L41

This paper has been typeset from a TEX/LATEX file prepared by the author.